

SCIENTIFIC REPORTS



OPEN

First evidence of denitrification vis-à-vis monsoon in the Arabian Sea since Late Miocene

Shubham Tripathi¹, Manish Tiwari¹, Jongmin Lee², Boo-Keun Khim² & IODP Expedition 355 Scientists[†]

Received: 08 November 2016

Accepted: 17 January 2017

Published: 21 February 2017

In the Arabian Sea, South Asian monsoon (SAM)-induced high surface water productivity coupled with poor ventilation of intermediate water results in strong denitrification within the oxygen minimum zone (OMZ). Despite the significance of denitrification in the Arabian Sea, we have no long-term record of its evolution spanning the past several million years. Here, we present the *first* record of denitrification evolution since Late Miocene (~10.2 Ma) in the Eastern Arabian Sea, where the SAM generates moderate surface water productivity, based on the samples retrieved during the International Ocean Discovery Program (IODP) Expedition 355. We find that (i) the SAM was persistently weaker from ~10.2 to 3.1 Ma; it did not intensify at ~8 Ma in contrast to a few previous studies, (ii) on tectonic timescale, both the SAM and the East Asian Monsoon (EAM) varied synchronously, (iii) the first evidence of denitrification and productivity/SAM intensification was at ~3.2–2.8 Ma that coincided with Mid-Pliocene Warm Period (MPWP), and (iv) the modern strength of the OMZ where denitrification is a permanent feature was attained at ~1.0 Ma.

Oxygen minimum zones (OMZs) - the regions of dissolved oxygen deficient ($O_2 < 20 \mu M$) water located in the tropical oceans - have been proposed to expand in the present scenario of global warming^{1,2}. OMZs play a significant role in producing N_2O - a powerful greenhouse gas through the process of denitrification (a process by which nitrate and nitrite are reduced to nitrogen gas) when the dissolved O_2 levels fall below $1 \mu M$ ³. A perennial OMZ develops between 150 and 1000 m water depth in the Arabian Sea due to various natural factors such as high surface water productivity and reduced ventilation of intermediate water⁴. The anoxic zones of these OMZs occupy only ~0.8% of the world ocean but are responsible for the highest production of N_2 through denitrification (~35% of the global production) out of which the Arabian Sea contributes the largest proportion (~17% of global N_2 production)⁵. The balance between nitrogen fixation and its removal through N_2 production is a key to carbon assimilation by primary production and CO_2 regulation in the atmosphere^{3,6}. In the Arabian Sea, most of the studies have examined denitrification variability over the past 100 kyr or younger; the longest record available goes back to 1 Ma in the Western Arabian Sea⁷. Hence, there is a lack of information regarding the long-term evolution of denitrification spanning the past several million years, especially from the Eastern Arabian Sea. Here, we examine samples from Site U1456 in the Eastern Arabian Sea retrieved during the IODP Expedition 355⁸ (Fig. 1).

To reveal the long-term OMZ variability and its coupling with surface water productivity, we analyzed multi-isotopic and geochemical proxies viz. nitrogen and carbon isotopic ratios ($\delta^{15}N$ and $\delta^{13}C$), total organic carbon and total nitrogen (TOC and TN) concentrations, and carbon to nitrogen (C/N) weight ratio of sedimentary organic matter (SOM).

Study Area

Site U1456 is located at $16^{\circ}37.28'N$, $68^{\circ}50.33'E$ in the Eastern Arabian Sea (EAS) (Fig. 1), ~475 km away from the Indian coast, and ~820 km from the modern mouth of the Indus River, and within the Laxmi Basin which is flanked by the Laxmi Ridge to the west and the Indian continental shelf to the east. The Laxmi Basin is characterized by a 200–250 km wide depression that runs in a northwest–southeast direction parallel to the west coast of India⁸. The site is situated at a water depth of 3640 m, which lies well above the modern lysocline (~3800 m)

¹National Centre for Antarctic and Ocean Research, Vasco-da-Gama, 403804, Goa, India. ²Department of Oceanography, Pusan National University, Busan, 46241, Korea. [†]A comprehensive list of consortium members appears at the end of the paper. Correspondence and requests for materials should be addressed to M.T. (email: manish@ncaor.gov.in) or B.-K.K. (email: bkchim@pusan.ac.kr)

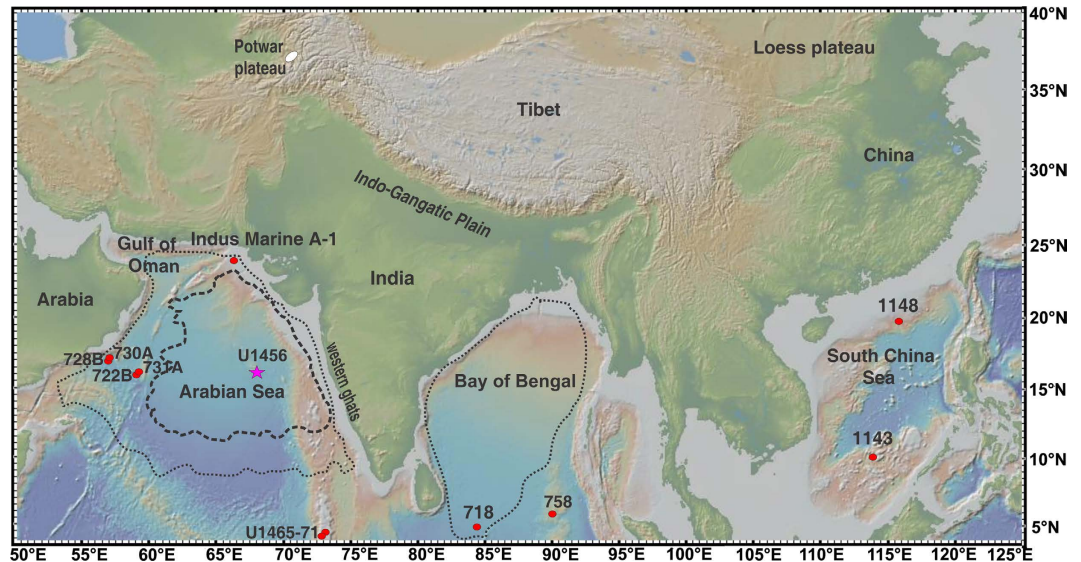


Figure 1. Locations of the IODP Expedition 355 Site U1456 in the Eastern Arabian Sea (3640 m of water depth, 16°37.28'N, 68°50.33'E) denoted by pink star⁸. The red circles represent ODP and IODP sites in the Arabian Sea^{7,27,28,29,32}, Bay of Bengal^{33,34} and South China Sea^{38,41}, which have been discussed in the present study. The white patch represents Potwar plateau³¹. The thin dotted curves in the Arabian Sea and the Bay of Bengal show modern anoxia¹ based on WOA2005 climatology. The thick black dotted curve in the Arabian Sea represents the approximate extent of denitrification zone⁴² (Figure created using GeoMapApp3.6.0, www.geomapapp.org).

in the Arabian Sea⁸. Three distinct water masses identified by Rochford⁹ in the Arabian Sea are Arabian Sea High Salinity Water (~50 m to 75 m) (ASHSW), Persian Gulf Water (~25 m to 70 m) (PGW), and Red Sea Water (~600 m to 900 m) (RSW)¹⁰. ASHSW shows greater seasonal variability than PGW and RSW and is considered as the main source of oxygen in the Western Arabian Sea (WAS)^{9,11}. Thus, the subsurface denitrification intensity in the WAS is controlled by the surface productivity as well as the supply of oxygen from the water masses¹¹. However, in the EAS, the subsurface denitrification is expected to be controlled mainly by the extent of surface productivity¹². An Argo float-based study in the Arabian Sea revealed the presence of high salinity water with inter-seasonal to inter-annual variability¹³. The vertical mixing of PGW and RSW between ~250 m to ~800 m result in the formation of the Arabian Sea Intermediate Water¹⁴. The deep water masses of the Indian Ocean comprise Antarctic Bottom Water (AABW), Circumpolar Deep Water (CDW), and Indian Deep Water (IDW). IDW forms in the Indian Ocean itself by the process of diffusion and upwelling and is characterised by low oxygen content and relatively enriched nutrients because of its aging¹⁵. The present-day bottom water in the Arabian Sea flows northward and upwells into the layer of North Indian Deep Water (~1500–3500 m)¹⁶.

Results and Discussion

The drilled section at Site U1456 is divided into four lithologic units based on a variety of sediment properties (Fig. 2a); Unit I (~121 m thick and Pleistocene nannofossil ooze interbedded with very thin turbidites), Unit II (~240 m thick and late Pliocene to early Pleistocene sand and silt), Unit III (~370 m thick and late Miocene to late Pliocene clay/claystone, sand/sandstone, nannofossil chalk, and nannofossil-rich claystone), and Unit IV (~380 m thick and older than late Miocene claystone, calcarenite, calcilutite, and conglomerate/breccia). These lithologies are characterized by different mineralogical and geochemical properties⁸.

Since the drilled core is very long (1109.4 m) and the site is quite deep (3640 m)⁸, the isotopic ratios of the SOM should be evaluated for the diagenetic alterations related to the lithology. Diagenesis of the organic matter begins within the photic zone of the water column, which continues during sinking. It further maintains unceasingly within the bioturbated mixed layer of sediment (a few cm to ~10 cm depth) and only a few percent (1 to 0.01%) of organic matter is finally buried/preserved in the sediment¹⁷. Although microbial activity has been found even up to several hundred meters deep into the sedimentary sequence¹⁸, diagenesis reduces significantly with increasing depth. Popp *et al.*¹⁹ suggested that despite the loss of organic matter due to remineralization, the $\delta^{13}\text{C}$ of SOM remains almost unchanged with increasing depth. Similarly, a very small $\delta^{15}\text{N}$ offset was found between core top sediments and sinking particles in the equatorial Pacific region; the loss of organic matter due to diagenesis in the upper section of the core top shows no corresponding $\delta^{15}\text{N}$ change¹¹. Core top studies from the Western Arabian Sea reported no correlation between TN and $\delta^{15}\text{N}$, which indicates that diagenesis does not affect $\delta^{15}\text{N}$ variation⁷. We also obtain no relationship between TN and $\delta^{15}\text{N}$ ($r^2 = 0.19$; Supplementary Fig. 1). Thus, diagenesis appears to cause no significant alteration in $\delta^{13}\text{C}$ and $\delta^{15}\text{N}$ values of SOM at Site U1456.

The C/N ratio of marine organic matter generally ranges from 8 to 10²⁰. Terrestrial organic matter predominantly consists of compounds like cellulose and lignin with much low nitrogen content. The C/N ratios of land-derived organic matter, therefore, are much high in the range between 20 and 100²⁰. The mean $\delta^{13}\text{C}$ values

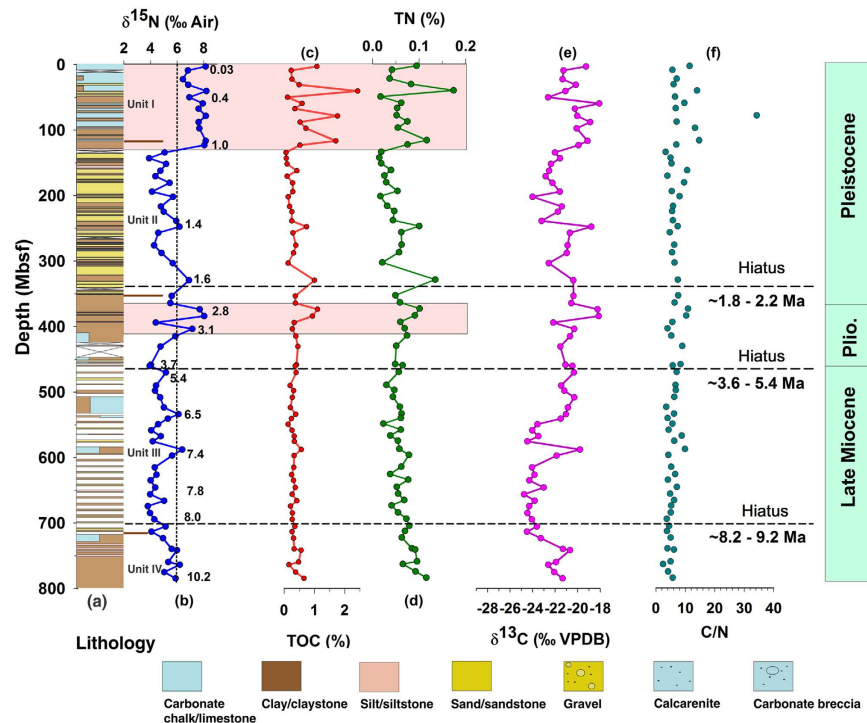


Figure 2. Record of denitrification, surface water productivity, and provenance of the Sedimentary Organic Matter (SOM) in the Eastern Arabian Sea since Late Miocene. (a) Lithostratigraphy of site U1456, (b) denitrification variability ($\delta^{15}\text{N}$ of SOM), (c,d) paleoproductivity variability (weight percent total organic carbon [TOC] and total nitrogen [TN] of SOM), (e,f) SOM provenance indicators ($\delta^{13}\text{C}$ and C/N ratio). The coloured, rectangular boxes show the intensified OMZ coupled with surface water productivity when denitrification occurred in the basin. The horizontal dotted lines indicate the position of the hiatuses. The vertical dashed line over panel 'b' show denitrification threshold and horizontal brown lines separates different lithological units. The age data (in Ma) at Site U1456, shown by the Indo-Arabic numerals in 'panel b', are based on calcareous nannofossil and planktonic foraminifera biostratigraphy, together with magnetostratigraphy⁸.

of the marine organic matter, C4, and C3 plants are about -21‰ , -13‰ , and -27‰ , respectively²¹. The C/N ratio together with $\delta^{13}\text{C}$ of SOM has been widely used to determine the origin of organic matter²⁰. At Site U1456, the $\delta^{13}\text{C}$ values vary from -18‰ to -25‰ and most of the C/N ratios range from 6 to 10, indicating that SOM is mostly of marine origin (Fig. 2e,f and Supplementary Fig. 2).

Based on surface sediment analysis of more than 100 locations in the Central and Eastern Arabian Sea (most of them are located in the Eastern Arabian Sea), the $\delta^{15}\text{N}$ values of SOM have been found to vary from 6‰ to 11‰ ²². In most of the oxygenated basins, the $\delta^{15}\text{N}$ values do not exceed 6‰ while those from the oxygen deficient basins are highly enriched with mostly higher than 6‰ ^{7,22,23,24}. Thus, the periods with $\delta^{15}\text{N}$ values higher than 6‰ may signify denitrification associated with strong OMZ. At Site U1456, the $\delta^{15}\text{N}$ values of SOM vary between 2.4‰ to 8.2‰ (Fig. 2b). The maximum TOC and TN values are 2.42% and 0.17% , respectively (Fig. 2c,d). The Mid- to Late Pliocene (~ 3.2 to 2.7 Ma) is characterized by high $\delta^{15}\text{N}$ values ($>6\text{‰}$) along with high TOC and TN values, indicating denitrification/strong OMZ (Fig. 2). Another period of denitrification/OMZ intensification ($\delta^{15}\text{N} > 6\text{‰}$) takes place from ~ 1.0 Ma to the core top (0.03 Ma) (Fig. 2b). During these periods of intense denitrification, the surface water productivity indicators viz. TOC and TN contents also represent an increasing trend (Fig. 2c,d). Intense wind-induced productivity and particle flux occur in the Arabian Sea during the monsoon seasons²⁵. Modern climatological chlorophyll *a* data show that the surface water productivity in the Eastern Arabian Sea is driven by both the summer and the winter monsoons²⁶. Thus, surface water productivity variability in the Eastern Arabian Sea is a manifestation of the SAM variability, which can be linked to denitrification/OMZ intensification.

The origin and evolution of the SAM are still a topic of debate. According to the previous hypothesis based on a study from the Western Arabian Sea (Ocean Drilling Program (ODP) Site 722), the initiation/intensification of the SAM occurred at around 8.5 Ma and continued until 6 Ma²⁷ (Fig. 3g). Another study from the same ODP Site 722 shows that the onset of the SAM took place at ~ 12.9 Ma and a major intensification occurred at ~ 7 Ma²⁸. In contrast, a decrease in *G. bulloides* abundance was found at 8.5 Ma (Fig. 3f) from the ODP Site 722 implying reducing SAM²⁹. A recent study from the inner seas of the Maldives (IODP sites U1465-71) postulates a proto-monsoon from 25 – 12.9 Ma and an abrupt increase in the monsoon at ~ 12.9 Ma³⁰ (Fig. 3d). The $\delta^{13}\text{C}$ values of paleosols from the Siwalik Group sediments in the northern Pakistan spanning the past 18 Myr showed a marked shift from C-3 to C-4 dominated plants at ~ 7.4 Ma, which may be associated with SAM inception and again the flood plains were mostly occupied by C-4 grassland in Plio-Pleistocene³¹ indicating monsoon

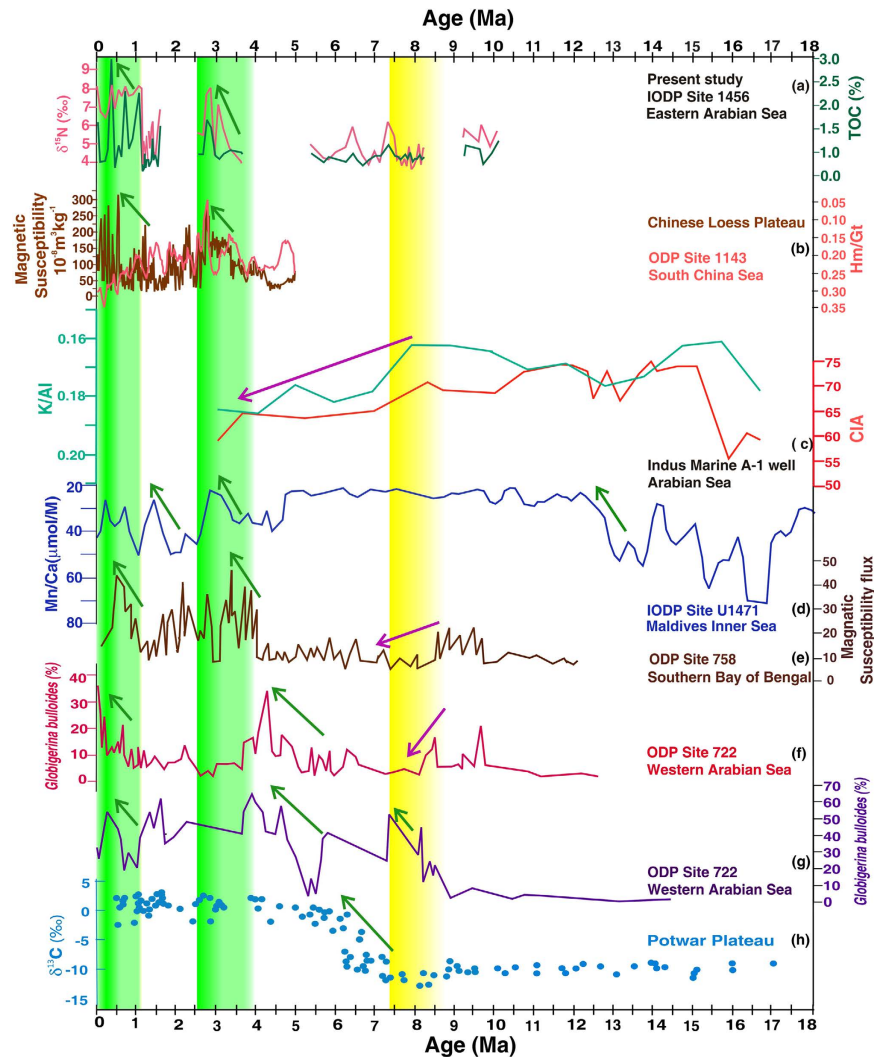


Figure 3. Comparative records of the South Asian Monsoon and East Asian Monsoon since Mid-Miocene. (a) $\delta^{15}\text{N}$ and total organic carbon (TOC) from IODP site U1456, (b) Magnetic susceptibility record³⁷ of Chinese loess plateau and Hm/Gt (40 point moving average) from the South China Sea ODP site 1143³⁸, (c) Chemical Index of Weathering (CIA) from the Indus river fan³², (d) Mn/Ca record from the Maldives inner sea³⁰ (e) Magnetic susceptibility record of the southern Bay of Bengal ODP site 758³⁴, (f) *G. bulloides* abundance from ODP site 722²⁹, (g) *G. bulloides* abundance from ODP site 722²⁷, and (h) $\delta^{13}\text{C}$ of calcrites from the Potwar Plateau³¹. The green arrows represent the strengthening of monsoon and the purple indicate the weakening of monsoon. The yellow band marks the arid period when many of the studies including the present study show the weakened monsoon while the green bands indicate the periods of strengthened monsoon.

intensification (Fig. 3h). Recent records of Himalayan weathering represented by the chemical index of alteration (CIA) and K/Al ratios (Fig. 3c) demonstrated that SAM attained the maximum strength at 15 Ma, remained high until 10.5 Ma, gradually weakened until ~3.5 Ma, and again increased from the Late Pliocene to Pleistocene³². The Sr isotope and clay mineral data also suggested weaker SAM after 8 Ma³³. Our record from Site U1456 spans ~10.2 to 0.03 Ma, but includes several hiatuses dated to ~8.2–9.2 Ma, ~3.7–5.4 Ma, and ~1.6–2.2 Ma⁸. Nevertheless, we interpret that surface water productivity in the Eastern Arabian Sea was low from 10.15 Ma to 3.2 Ma as evident from uniformly low values of TOC and TN (3a and 2b). Additionally, during this period, the $\delta^{15}\text{N}$ did not reach the threshold value (~6‰) indicative of denitrification (Fig. 3a). This implies that neither the surface water productivity (TOC, TN) nor the OMZ intensity supports any major intensification in SAM strength from ~10 to ~3.2 Ma, which is also documented in the different regions (the South China Sea, the Northern Arabian Sea and the Bay of Bengal)^{32,34}. These studies^{32,34} reported that SAM and EAM were reduced more or less in parallel albeit with a time-lag; the EAM started declining at ~10 Ma while the SAM began decreasing at ~8 Ma. But, we find that the SAM was weak at ~10 Ma indicating that EAM and SAM varied in consonance, without any apparent time lag, on tectonic timescale. This Late Miocene reduction in monsoon strength could be a result of global cooling after the Middle Miocene Climatic Optimum³⁵. At around 8 Ma, $\delta^{15}\text{N}$ values vary between 3.7‰ to 5.8‰, i.e., the OMZ was not intense enough to cause denitrification and the surface water productivity was diminished (Figs 2 and 3a), which implies that SAM did not intensify at ~8 Ma.

During the study period, for the first time, the OMZ intensified to the level that denitrification takes place was at ~3.2–2.8 Ma (Fig. 2b). During this period, the surface water productivity (Fig. 2c,d) was also enhanced, indicating stronger SAM, which coincides with MPWP³⁶. Earlier studies, based on magnetic susceptibility (Chinese Loess Plateau, Fig. 3b; southern Bay of Bengal, Fig. 3e) and hematite to goethite ratio (Hm/Gt, South China Sea, Fig. 3b), also reported the enhanced SAM and EAM during ~3.6–2.6 Ma^{34,37,38}. A new magnetostratigraphy study from Chinese Loess Plateau spanning from ~8.2 Ma to 2.6 Ma documented long-term East Asian Summer Monsoon (EASM) intensification. Both proxy, as well as numerical climate model assessment, show that the Antarctic glaciation was an important driver for the long-term trend of late Miocene-Pliocene EASM intensification³⁹. To examine the responsible mechanisms, a modeling experiment, using the NCAR climate model CCM3, with idealized Himalayan-Tibetan Plateau elevations explains the observed increase of the EAM as a result that the Himalayan-Tibetan Plateau attained modern extension along its eastern and northern margins³⁴. It was speculated that it might not have affected the SAM circulation pattern³⁴. The present study, based on the multi-proxy records, suggests that the SAM was also enhanced in parallel with the EAM and therefore the intensification can be ascribed to the same mechanism. A recent review⁴⁰ investigated the role of the Tibet Plateau in affecting SAM, and found that it simply acts as a physical barrier for northerly cool, dry winds. Its role as an elevated heat source is of secondary importance in affecting the SAM. EAM dynamics is also affected by the Tibet Plateau, which is located in the path of subtropical jet streams⁴⁰. The increase in both the EAM and SAM during ~3.6–2.6 Ma could have resulted in the increased weathering and organic carbon burial, as evident by higher TOC (Fig. 2c), leading to atmospheric CO₂ drawdown that would have possibly contributed to Northern Hemisphere Glaciation (NHG) at 2.7 Ma⁴⁰. Thereafter, from 2.8 Ma to ~1.0 Ma, $\delta^{15}\text{N}$ values as well as the surface water productivity declined in parallel, indicating relatively weaker SAM. Previous studies also reported the weakened EAM and SAM after ~2.6 Ma^{34,36,37}, confirming our results, which coincides with the onset of NHG. Finally, the OMZ reached its modern strength, i.e., denitrification became a permanent feature, at about ~1.0 Ma closely following the enhanced surface water productivity. It implies that SAM intensified from ~1.0 Ma as reported in earlier studies viz. the enhanced sedimentation rate in the Indus Fan³², the increased chemical weathering from the Bengal Fan³³ and the South China Sea⁴¹, the rise of magnetic susceptibility (Fig. 3b) and mean sediment flux from the Indian Ocean³⁸.

Methods

The samples used in the present study were obtained onboard the *JOIDES Resolution*. 5–15 cm long whole-round core sections at the interval of every core or every alternate core were squeezed using titanium steel squeezing device to obtain the interstitial water. The remaining sediments are named 'squeeze cake'. The samples were dried to remove the moisture at 45 °C before processing. Around 10 to 20 g of sediment aliquots were taken for further analysis. Dried samples were finely grounded for homogenization. Homogeneous samples were divided into two batches for geochemical and isotopic analyses - (i) 2 N HCl treatment for total organic carbon (TOC) and $\delta^{13}\text{C}$ measurement and (ii) untreated for determination of total nitrogen (TN) content and $\delta^{15}\text{N}$ values. 20 ml of 2 N HCl solution was added to 5–10 g of fine sediment powder. The mixture was shaken mechanically and allowed to stand for ~12 hours. The sample was then washed with ultrapure demineralized water and approximately 25 mg of treated sample was used for TOC and $\delta^{13}\text{C}$ analysis. For TN and $\delta^{15}\text{N}$ measurement, approximately 40 mg of bulk ground sediment was used. The $\delta^{15}\text{N}$ and $\delta^{13}\text{C}$ values were determined using isotope ratio mass spectrometer coupled with an element analyzer at Marine Stable Isotope Lab, National Centre for Antarctic and Ocean Research, Goa, India and Department of Oceanography, Pusan National University, Busan, Korea. The standard used was ammonium sulfate (IAEA-N-1) and cellulose (IAEA-CH-3). The analytical precision for $\delta^{15}\text{N}$ and $\delta^{13}\text{C}$ is $\pm 0.12\%$ and $\pm 0.06\%$, respectively. Similarly, TN and TOC were determined using sulfanilamide as the standard. The analytical precision for TN and TOC is $\pm 0.63\%$ and $\pm 0.84\%$, respectively.

Data Availability. The data used in this study are included in the supplementary information files.

References

- Paulmier, A. & Ruiz-Pino, D. Oxygen minimum zones (OMZs) in the modern ocean. *Prog. Oceanogr.* **80**, 113–128 (2009).
- Stramma, L. *et al.* Ocean oxygen minima expansions and their biological impacts. *Deep-Sea Res.* **157**, 587–595 (2010).
- Bange, H. W. *et al.* Nitrous oxide emissions from the Arabian Sea: A synthesis. *Atmos. Chem. Phys.* **1**, 61–71 (2001).
- Naqvi, S. W. A. *et al.* Marine hypoxia/anoxia as a source of CH₄ and N₂O. *Biogeosciences* **7**, 2159–2190 (2010).
- Ward, B. B. *et al.* Denitrification as the dominant nitrogen loss process in the Arabian Sea. *Nature* **461**, 78–81 (2009).
- Altabet, M. A., Higginson, M. J. & Murrey, D. W. The effect of millennial-scale changes in Arabian Sea denitrification on Atmospheric CO₂. *Nature* **415**, 159–162 (2002).
- Altabet, M. A., Murray, D. W. & Prell, W. L. Climatically linked oscillations in Arabian Sea denitrification over the past 1 m.y.: Implications for the marine N cycle. *Paleoceanography* **14**, 732–743 (1999).
- Pandey, D. K., Clift, P. D., Kulhanek, D. K. & The Expedition 355 Scientists. Site 1456. In *The Proceedings of the International Ocean Discovery Program* **355**, 1–61, doi: 10.14379/iodp.proc.355.103.2016 (2016).
- Rochford, D. J. Salinity maximum in the upper 100 meters of the north Indian Ocean. *Aust. J. Mar. Freshwater. Res.* **15**, 1–24 (1964).
- Prasanna, K. S. & Prasad, T. G. Formation and spreading of Arabian Sea high-salinity water mass. *Journal of Geophysical Research.* **104**, 1455–1464 (1999).
- Altabet, M. A., Francois, R., Murray, D. W. & Prell, W. L. Climate related variations in denitrification in the Arabian Sea from sediment ¹⁵N/¹⁴N ratios. *Nature*. **373**, 506–509 (1995).
- Agnihotri, R., Bhattacharya, S. K. & Sarin, M. M. Changes in surface productivity, sub-surface denitrification and SW monsoon during the Holocene: A multi proxy record from the eastern Arabian Sea. *The Holocene* **13**(5), 701–713 (2003).
- Chowdary, J. S., Gnanaseelan, C., Thompson, B. & Salvekar, P. S. Water mass property and transports in the Arabian Sea from Argo Observations. *Journal of Atmospheric & Ocean Science* **10**, 235–260 (2007).
- Premchand, K., Sastry, J. S. & Murty, C. S. Water mass structure in the Western Indian Ocean- Part 2: The spreading and transformation of the Persian Gulf Water. *Mausam* **37**, 179–186 (1986).
- Tally, L. D., Pickard, G. L., Emery, W. J. & Swift, J. H. Descriptive physical oceanography: An Introduction. Elsevier, China, 387–399 (2012).
- Shetye, S. R., Gouveia, A. D. & Shenoi, S. S. C. Circulation and water masses of the Arabian Sea. *Proc. Indian Acad. Sci.* **103**, 107–123 (1994).

17. Rullkötter, J. Organic matter: driving force for early diagenesis. In (ed. Schulz, H. D., Zabel, M.) *Marine geochemistry*, Springer, Berlin, 125–206 (2006).
18. Parkes, J. R. *et al.* Deep bacterial biosphere in Pacific Ocean sediments. *Nature* **371**, 410–413 (1994).
19. Popp, B. N., Parekh, P., Tilbrook, B., Bidigare, R. R. & Laws, E. A. Organic carbon variation in sedimentary rocks as chemostratigraphic and paleoenvironmental tools. *Palaeogeogr. Palaeoclimat. Palaeoecol.* **132**, 119–132 (1997).
20. Meyers, P. A. Preservation of elemental and isotopic source identification of sedimentary organic matter. *Chem Geol.* **114**, 289–302 (1994).
21. Farquhar, G. D., Ehleringer, J. R. & Hubick, K. T. Carbon isotope discrimination and photosynthesis. *Ann. Rev. Plant Physiol. Plant Mol. Biol.* **40**, 503–537 (1989).
22. Gaye-Haake, B. *et al.* Stable nitrogen isotopic ratios of sinking particles and sediments from the northern Indian Ocean. *Mar. Chem.* **96**, 243–255 (2005).
23. Ganeshram, R. S., Pedersen, T. F., Calvert, S. E. & Murray, J. W. Large changes in oceanic nutrient inventories from glacial to interglacial periods. *Nature* **376**, 755–758 (1995).
24. Liu, K. & Kaplan, I. R. The eastern tropical Pacific as a source of ¹⁵N-enriched nitrate in seawater off southern California. *Limnol. Oceanogr.* **34**, 820–830 (1989).
25. Nair, R. R. *et al.* Increased particle flux to the deep ocean related to monsoon. *Nature* **338**, 749–751 (1989).
26. Cabarcos, E., Flores, J. A., Singh, A. D. & Sierro, F. J. Monsoonal dynamics and evolution of the primary productivity in the eastern Arabian Sea over the past 30 ka. *Palaeogeogr. Palaeoclimat. Palaeoecol.* **411**, 249–256 (2014).
27. Kroon, D., Steens, T. N. F. & Troelstra, S. R. Onset of monsoonal related upwelling in the western Arabian Sea. In: Prell, W. L. *et al.* (eds) *Proceedings of the ODP Sci. Results.* **117**, 257–264 (1991).
28. Gupta, A. K., Yuvaraja, A., Prakasam, M., Clemens, S. C. & Velu, A. Evolution of the South Asian monsoon wind system since the late Middle Miocene. *Palaeogeogr. Palaeoclimat. Palaeoecol.* **438**, 160–167 (2015).
29. Huang, Y., Clemens, S. C., Liu, W., Wang, Y. & Prell, W. L. Large-scale hydrological change drove the late Miocene C4 plant expansion in the Himalayan foreland and Arabian Peninsula. *Geology* **35**, 531–534 (2007).
30. Betzler, C. *et al.* The abrupt onset of the modern South Asian Monsoon winds. *Sci. Rep.* **6**, 29838 (2016).
31. Quade, J., Cerling, T. E. & Bowman, J. R. Development of Asian monsoon revealed by marked ecological shift during the latest Miocene in northern Pakistan. *Nature* **342**, 163–165 (1989).
32. Clift, P. D. *et al.* Correlation of Himalayan exhumation rates and Asian monsoon intensity. *Nature geoscience* **1**, 875–880 (2008).
33. Derry, L. A. & France-Lanord, C. Neogene Himalayan weathering history and river ⁸⁷Sr/⁸⁶Sr: impact on the marine Sr record. *Earth Planet. Sci. Lett.* **142**, 59–74 (1996).
34. An, Z., Kutzbach, J. E., Prell, W. L. & Porter, S. C. Evolution of Asian monsoons and phased uplift of the Himalaya-Tibetan plateau since Late Miocene times. *Nature* **411**, 62–66 (2001).
35. Zachos, J., Pagani, M., Salon, L., Thomas, E. & Billups, K. Trends, rhythms and aberrations in global climate 65 Ma to Present. *Science* **292**, 686–693 (2001).
36. Haywood, A. M., Dowsett, H. J. & Dolan, A. M. Integrating geological archives and climate models for the mid-Pliocene warm period. *Nature communications* **7**, 1–14, doi: 10.1038/ncomms10646 (2016).
37. Sun, Y., Lu, H. & An, Z. Grain size of loess, palaeosol and Red Clay deposits on the Chinese Loess Plateau: Significance for understanding pedogenic alteration and palaeomonsoon evolution. *Palaeogeogr. Palaeoclimat. Palaeoecol.* **241**, 129–138 (2006).
38. Zhang, Y. G., Ji, J., Balsam, W., Liu, L. & Chen, J. Mid-Pliocene Asian monsoon intensification and the onset of Northern Hemisphere glaciation. *Geology* **37**, 599–602 (2009).
39. Ao, H., Roberts, A. P., Dekkers, M. J., Liu, X., Rohling, E. J., Shi, Z., An, Z. & Zhao, X. Late Miocene–Pliocene Asian monsoon intensification linked to Antarctic ice-sheet growth. *Earth Planet. Sci. Lett.* **444**, 75–87 (2016).
40. Molnar, P., Boos, W. R. & Battisti, D. S. Orographic Controls on Climate and Paleoclimate of Asia: Thermal and Mechanical Roles for the Tibetan Plateau. *Annu. Rev. Earth Planet. Sci.* **38**, 77–102 (2010).
41. Wang, P. *et al.* Site 1148. Proc. Ocean Drill. Prog. *Init. Rep.* **184**, 121 (2000).
42. Naqvi, S. W. A. Geographical extent of denitrification in the Arabian Sea in relation to some physical processes. *Oceanol. Acta* **14**, 281–290 (1991).

Acknowledgements

This research used samples and data provided by IODP, collected onboard the vessel *JOIDES Resolution* (IODP Expedition 355-Arabian Sea Monsoon). M.T. and S.T. thank the Secretary, Ministry of Earth Sciences (MoES), Govt. of India and Director, National Centre for Antarctic and Ocean Research (NCAOR) for support and encouragement (NCAOR Contribution no. 03/2017). B.K.K. and J.L. appreciate the National Research Foundation of Korea grant (2016R1A2B4008256) and K-IODP program by the Korea government. This research has also been supported by the Research Council of Norway (RCN) and MoES, Govt. of India through the Ind-Nor programme (grant No. 248793 and MoES/Ind-Nor/PS-8/2015). We also thank the anonymous reviewers and the editor for constructive comments that helped to improve the manuscript.

Author Contributions

M.T. and B.K.K. designed the research and collected the samples onboard *JOIDES Resolution* aided by IODP Expedition 355 Scientists; S.T. and J.L. did the sample processing and analysis; S.T. and M.T. supported by B.K.K. and J.L. wrote the manuscript, which was edited by all the IODP Expedition 355 Scientists.

Additional Information

Supplementary information accompanies this paper at <http://www.nature.com/srep>

Competing financial interests: The authors declare no competing financial interests.

How to cite this article: Tripathi, S. *et al.* First evidence of denitrification vis-à-vis monsoon in the Arabian Sea since Late Miocene. *Sci. Rep.* **7**, 43056; doi: 10.1038/srep43056 (2017).

Publisher's note: Springer Nature remains neutral with regard to jurisdictional claims in published maps and institutional affiliations.



This work is licensed under a Creative Commons Attribution 4.0 International License. The images or other third party material in this article are included in the article's Creative Commons license, unless indicated otherwise in the credit line; if the material is not included under the Creative Commons license, users will need to obtain permission from the license holder to reproduce the material. To view a copy of this license, visit <http://creativecommons.org/licenses/by/4.0/>

© The Author(s) 2017

Consortia

IODP Expedition 355 Scientists:

Dhananjai K. Pandey¹, Peter D. Clift³, Denise K. Kulhanek⁴, Sergio Andò⁵, James A.P. Bendle⁶, Sophia Aharonovich⁷, Elizabeth M. Griffith⁸, Gundiga P. Gurumurthy⁹, Annette Hahn¹⁰, Masao Iwai¹¹, Anil Kumar¹², A. Ganesh Kumar¹³, Hannah M. Liddy¹⁴, Huayu Lu¹⁵, Mitchell W. Lyle¹⁶, Ravi Mishra¹, Tallavajhala Radhakrishna¹⁷, Claire M. Routledge¹⁸, Rajeev Saraswat¹⁹, Rakesh Saxena²⁰, Giancarlo Scardia²¹, Girish K. Sharma²², Arun D. Singh²³, Stephan Steinke²⁴, Kenta Suzuki²⁵, Lisa Tauxe²⁶, Zhaokai Xu²⁷, Zhaojie Yu²⁸.

³Department of Geology and Geophysics, Louisiana State University, E253 Howe-Russell-Kniffen, Geoscience Complex, Baton Rouge, LA 70803, USA.

⁴International Ocean Discovery Program, Texas A&M University, 1000 Discovery Drive College Station TX 77845, USA.

⁵Department of Earth and Environmental Sciences, University of Milano Bicocca, Piazza della Scienza 4, 20126 Milan, Italy.

⁶School of Geography, Earth and Environmental Sciences, University of Birmingham, Edgbaston, Birmingham B15 2TT United Kingdom.

⁷Department of Earth and Planetary Sciences, Faculty of Science and Engineering, Macquarie University Level 2, The Australian Hearing Hub, 16 University Avenue, Sydney NSW 2109, Australia.

⁸Department of Earth and Environmental Sciences, University of Texas at Arlington, Geosciences Building, Room 107, 500 Yates Street, Arlington TX 76019 USA.

⁹Manipal Centre for Natural Sciences, Manipal University, Dr. T.M.A. Pai Planetarium Building, Manipal 576104, India.

¹⁰MARUM, University of Bremen, Leobener Strasse 28359 Bremen, Germany.

¹¹Center for Advanced Marine Core Research/Natural Science Cluster, Kochi University, 2-5-1 Akebono-cho, Kochi 780-8520, Japan.

¹²Wadia Institute of Himalayan Geology, 33 GMS Road, Dehradun Uttarakhand 248001, India.

¹³Marine Biotechnology Department, National Institute of Ocean Technology, Velachery-Tambaram Main Road Pallikaranai, Chennai 600100, India.

¹⁴Department of Earth Sciences, University of Southern California, 3651 Trousdale Parkway Los Angeles CA 90089, USA.

¹⁵School of Geographical and Oceanographical Sciences, Nanjing University, 163 Xianlin Avenue, Nanjing 210023, China.

¹⁶College of Earth, Ocean and Atmospheric Sciences, Oregon State University, 104 CEOAS Administration Building, Corvallis OR 97331 USA.

¹⁷Geosciences Division, National Centre for Earth Science Studies, Aakkulam, Trivandrum 695031, India.

¹⁸University College London, Gower Street, London WC1E 6BT, United Kingdom.

¹⁹Geological Oceanography Division, National Institute of Oceanography, Dona Paula, Goa 403004, India.

²⁰ONGC 11 High, Bandra-Sion Link Road, Mumbai 400017, India.

²¹Instituto de Geociências e Ciências Exatas, Universidade Estadual Paulista, 1515 Avenida 24-A Rio Claro SP 13506-900, Brazil.

²²Department of Geology, Kumaun University, Nainital 263002, India.

²³Department of Geology, Banaras Hindu University, Varanasi, Uttar Pradesh 221005, India.

²⁴Department of Geological Oceanography, College of Ocean and Earth Sciences, Xiamen University, Xiping Building, Xiang'an South Road, Xiang'an District, Xiamen 361102, China.

²⁵Graduate School of Environmental Science, Hokkaido University, N10W5, Kita-ku Sapporo 060-0810, Japan.

²⁶Scripps Institution of Oceanography, 9500 Gilman Drive, La Jolla CA 92093-0220, USA.

²⁷Key Laboratory of Marine Geology and Environment, Institute of Oceanology, Chinese Academy of Sciences 7 Nanhai Road, Qingdao Shandong 266071, China.

²⁸Laboratoire Géosciences Paris-Sud (GEOPS, UMR8148-CNRS) Université de Paris-Sud (Orsay) Bâtiment 504 91405, Orsay Cedex, France.